*Geological Magazine*

**www.cambridge.org/geo**

# *In situ* rare earth element analysis of a lower Cambrian phosphate nodule by LA-ICP-MS

Yun-Tao Ye[1], Hua-Jian Wang[1], Xiao-Mei Wang[1], Li-Na Zhai[2], Chao-Dong Wu[3,4] and Shui-Chang Zhang[1]

[1]Key Laboratory of Petroleum Geochemistry, Research Institute of Petroleum Exploration and Development, China National Petroleum Corporation, Beijing 100083, China; [2]Key Laboratory of Marine Geology and Environment, Institute of Oceanology, Chinese Academy of Sciences, Qingdao 266071, China; [3]Key Laboratory of Orogenic Belts and Crustal Evolution, Ministry of Education, School of Earth and Space Sciences, Peking University, Beijing 100871, China and [4]Institute of Oil and Gas, Peking University, Beijing 100871, China

**Original Article**

**Cite this article:** Ye Y-T, Wang H-J, Wang X-M, Zhai L-N, Wu C-D, and Zhang S-C (2021) *In situ* rare earth element analysis of a lower Cambrian phosphate nodule by LA-ICP-MS. *Geological Magazine* **158**: 749–758. https://doi.org/10.1017/S0016756820000850

Received: 29 September 2019
Revised: 7 July 2020
Accepted: 10 July 2020
First published online: 4 September 2020

**Keywords:**
Carbonate fluorapatite; cerium anomaly; MREE enrichment; stratified ocean; Niutitang Formation

**Author for correspondence:**
Hua-Jian Wang,
Email: wanghuajian@petrochina.com.cn

## Abstract

Rare earth elements (REE) in marine minerals have been widely used as proxies for the redox status of depositional and/or diagenetic environments. Phosphate nodules, which are thought to grow within decimetres below the sediment–water interface and to be able to scavenge REE from the ambient pore water, are potential archives of subtle changes in REE compositions. Whether their REE signals represent specific redox conditions or they can be used to track the overlying water chemistry is worth exploring. Through *in situ* laser ablation – inductively coupled plasma – mass spectrometry (LA-ICP-MS), we investigate the REE compositions of a drill-core-preserved phosphate nodule from the lower Cambrian Niutitang Formation in the Daotuo area, northeastern Guizhou Province, South China. REE distributions of the nodule show concentric layers with systematic decreases in Ce anomalies (Ce/Ce*) from the core to the rim. The lowest Ce/Ce* appears in the outer rim where REE concentrations are relatively high. These results are interpreted to reflect REE exchange with pore water at a very early stage or bathymetric variation during apatite precipitation. The origin of the shale-normalized middle REE (MREE) enrichment in our sample is less constrained. Possible driving factors include preferential MREE substitution for Ca in the apatite lattice, degradation of organic matter and deposition beneath a ferruginous zone. Although speculative, the last possibility is consistent with the chemically stratified model for early Cambrian oceans, in which dynamic fluctuations of the chemocline provided an ideal depositional context for phosphogenesis.

## 1. Introduction

Rare earth elements (REE) are reliable geochemical tracers and have been used successfully in oceanographic studies of redox conditions. Significantly, because of the substitution of REE for Ca, marine carbonates and phosphate particulates are often considered to be the archives of seawater or pore-fluid REE signals (Jarvis *et al.* 1994; Shields & Stille, 2001; Jiang *et al.* 2007; Hood & Wallace, 2015; Tostevin *et al.* 2016*b*; Wallace *et al.* 2017; Zhu & Jiang, 2017). However, because of the complexity of the controlling factors involved in this process, interpretations without careful assessment can be equivocal. Earlier studies usually utilized a leaching procedure to extract the REE. However, Tostevin *et al.* (2016*a*) recently proved that this method might be compromised by clay or Fe oxide contaminations during digestion. An alternative approach is to use laser ablation – inductively coupled plasma – mass spectrometry (LA-ICP-MS) to directly analyse solid samples. The advantages of LA-ICP-MS analysis include comparatively easy measurements of multiple elements with low detection limits and the ability to determine micrometric trace-element variations that are undetectable in bulk-rock analyses. In fact, LA-ICP-MS has been demonstrated to be a powerful tool in understanding the superposition of geological events, the formation of mineral deposits and even several fundamental questions concerning the evolution of the Earth system (Bright *et al.* 2009; Large *et al.* 2014; Auer *et al.* 2017; Wallace *et al.* 2017; Zhou *et al.* 2017; Zhu *et al.* 2019).

The goal of this study is to evaluate the effectiveness of using LA-ICP-MS for REE analysis of a lower Cambrian phosphate nodule preserved in a drill core from the Daotuo manganese deposit in Songtao County, northeastern Guizhou, South China. To our knowledge, this is the first lower Cambrian nodule reported from core material, which minimizes the influence of surface weathering. Previous geological and geochronological investigations of South China have provided an ideal framework for the P-enriched Niutitang Formation, such as the identification of the depositional condition and palaeolatitude (Chen *et al.* 2015*a*; Yeasmin *et al.* 2017). Here, we emphasize that a combination of *in situ* LA-ICP-MS mapping



CAMBRIDGE UNIVERSITY PRESS

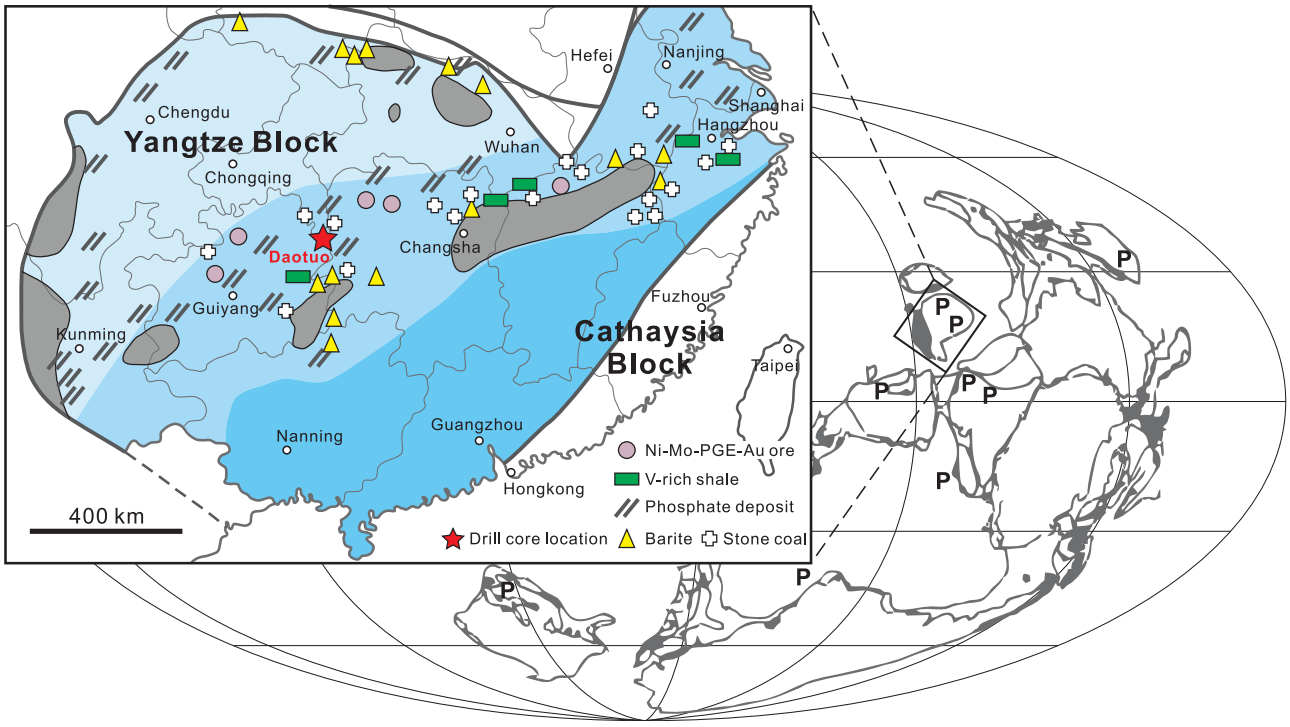


**Fig. 1.** (Colour online) Palaeogeographic map showing the distribution of various ore deposits on the Yangtze Block during early Cambrian time (McKerrow *et al.* 1992; Lehmann *et al.* 2016; Yeasmin *et al.* 2017). P – phosphorite.

and quantitative LA-ICP-MS spot analyses can provide unique information to determine the evolutionary history of a target.

## 2. Geological setting

The South China Craton, which consists of the Yangtze and Cathaysia blocks, developed a thick succession of well-studied Neoproterozoic and lower Cambrian strata (Wang & Li, 2003; Figs 1, 2). Palaeogeographic reconstruction of the upper Ediacaran Yangtze Block has revealed three sedimentary facies: (1) the shallow platform in the NW composed of carbonate layers of thickness > 100 m (the Dengying Formation); (2) the equivalent deep-water basin in the SE represented by the Liuchapo/Laobao cherts; and (3) a transitional slope characterized by mixed lithologies (Fig. 1; Steiner *et al.* 2007). During early Cambrian time, the platform setting suffered widespread drowning and it subsequently evolved into a muddy shelf (Yeasmin *et al.* 2017). The Niutitang Formation, which overlies the Dengying/Liuchapo Formation, is dominated by high total organic carbon (TOC) (up to 15%) black shales (Zhai *et al.* 2016). This black shale sequence also hosts discontinuous phosphate nodule, barite, Ni–Mo–PGE (platinum-group elements)–Au sulphide and V-rich deposits (Xu *et al.* 2011; Lehmann *et al.* 2016). The polymetallic unit was once considered to be close to the Ediacaran–Cambrian boundary (Horan *et al.* 1994; Mao *et al.* 2002), but more recent radiometric ages of 532.3 ± 0.7 Ma (Jiang *et al.* 2009), 522.7 ± 4.9 Ma (Wang *et al.* 2012), 522.3 ± 3.7 Ma and 524.2 ± 5.1 Ma (Chen *et al.* 2015*a*) from tuff beds at the base of the Niutitang Formation suggest that the polymetallic sulphide ore is much younger. Xu *et al.* (2011) reported an Re–Os age of 521 ± 5 Ma for the polymetallic unit, which agrees well with the biostratigraphic Tommotian stage (or Stage 2–3). Stratigraphically downward, U–Pb ages of 536.3 ± 5.5 Ma (Chen *et al.* 2009), 542.1 ± 5.0 Ma and 542.6 ± 3.7 Ma (Chen *et al.* 2015*a*) from the underlying Liuchapo Formation shift the position of the Ediacaran–Cambrian boundary within the Liuchapo Formation.

The Daotuo drill site, where we obtained the nodule sample, is located in Songtao County, *c.* 90 km NW of Tongren City (Fig. 1). The core covers a complete succession from the Sturtian-aged Tiesi'ao Formation to the lower Cambrian Bianmachong Formation. The phosphate nodule investigated in this study was preserved in the basal part of the Niutitang Formation, just below the polymetallic sulphide ore horizon (Figs 2, 3).

## 3. Methods

LA-ICP-MS was used to provide both imaging of the nodule and core-to-rim quantitative spot analysis. The REE contents were quantitatively measured at the Ministry of Education, Key Laboratory of Orogenic Belts and Crustal Evolution, School of Earth and Space Sciences, Peking University. The instruments used include a 193-nm excimer LA system (COMPexPro 102) and an Agilent 7500ce ICP-MS. Masses of $^{139}$La, $^{140}$Ce, $^{141}$Pr, $^{146}$Nd, $^{147}$Sm, $^{153}$Eu, $^{157}$Gd, $^{159}$Tb, $^{163}$Dy, $^{165}$Ho, $^{166}$Er, $^{169}$Tm, $^{172}$Yb and $^{175}$Lu were determined and calibrated through internal standardization of $^{43}$Ca, assuming 48.02% CaO (Jarvis *et al.* 1994). The NIST 610 standard was used as a reference. Although this NIST glass is not matrix matched to the phosphate sample, it offers evident advantages compared with various matrix-matched materials (Auer *et al.* 2017). Two other quality-control standards were analysed: NIST 612 and NIST 614. In total, 66 and 67 spots (60 μm in size) in the horizontal and vertical directions of the oval nodule were ablated, respectively. The GLITTER software (version 4.4.2) was used to obtain time-averaged REE concentrations. Reference materials ran alongside the samples were within 10% of the reported values for each element.

https://doi.org/10.1017/S0016756820000850 Published online by Cambridge University Press

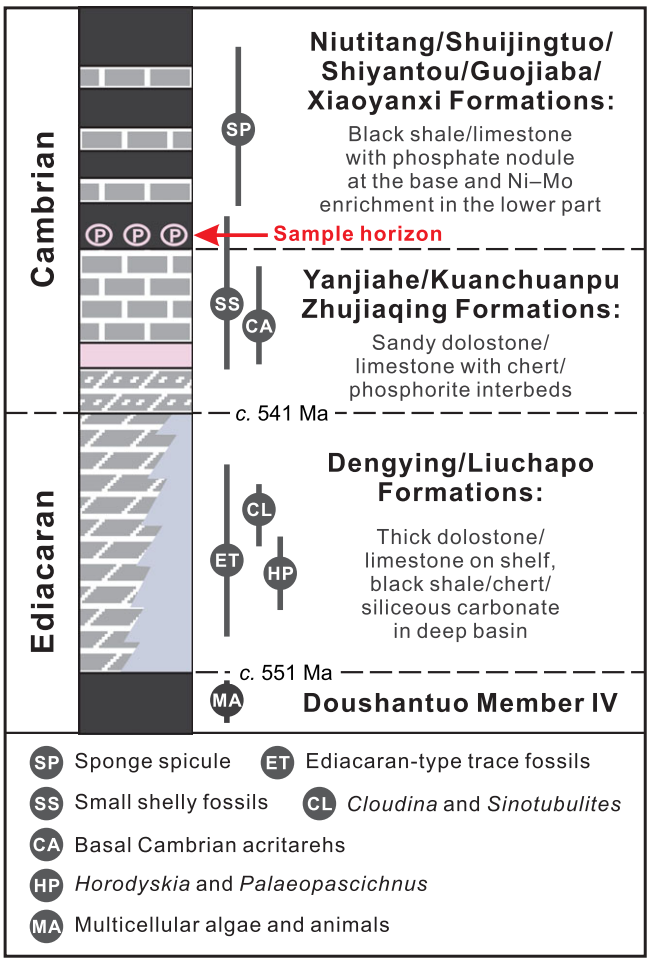


**Fig. 2.** (Colour online) Generalized litho- and bio-stratigraphy of the upper Ediacaran–lower Cambrian strata in South China (Wang *et al.* 2012).

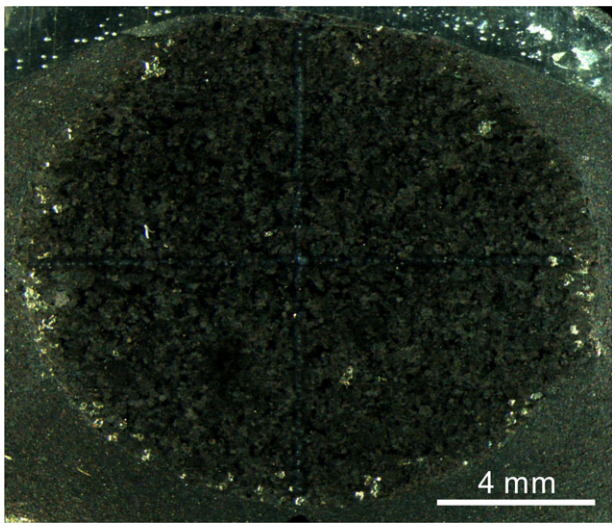


**Fig. 3.** (Colour online) Phosphate nodule thin-section under reflected light.

The resulting REE abundances were normalized to Post-Archaean Average Shale (PAAS; Taylor & McLennan, 1985) to remove the odd–even effect of element distributions and to produce curves in which enrichments and depletions are apparent. Because of excess La in seawater, the conventional Ce/Ce* calculation, $Ce/Ce^* = 2Ce_N/(La_N + Pr_N)$, can lead to incorrect Ce anomalies. The Ce/Ce* values presented here were therefore calculated geometrically by extrapolating back from Pr and Nd, that is, $Ce/Ce^* = Ce_N/(Pr_N \times Pr_N/Nd_N)$, as suggested by Lawrence *et al.* (2006).

The imaging experiment was conducted at the Key Laboratory of Petroleum Geochemistry, Research Institute of Petroleum Exploration and Development, using an Analyte Excite 193-nm excimer LA system coupled with an iCAP Q ICP-MS. A detailed description of the operating parameters can be found in Wang *et al.* (2016), including the laser energy, spot size, scan rate, gas flow and radio frequency power. LA-ICP-MS imaging of an approximately 0.9 $cm^2$ area covering one-quarter of the total nodule was obtained to display two-dimensional maps of element distributions. The raw LA-ICP-MS data were evaluated by means of factor analysis to assess the inter-element relationships. After calibration of variables and extraction of principal components, the factor axes were optimized using the Varimax rotation method.

## 4. Results

As illustrated in Figure 4, the LA-ICP-MS mapping reveals that the nodule is highly enriched in Ca, P, Sr and REE, but is depleted in Al, Si, Sc, Ti and Zr compared with its shale matrix. Notably, the REE distributions exhibit a concentric structure with moderate REE contents in the inner zone and elevated levels in the outer zone. Other elements – Fe, S, As and Se – are only concentrated between the nodule and the surrounding shale. Factor analysis of the raw LA-ICP-MS dataset led to the extraction of three components, explaining 64.1% of the total variance (Fig. 5; online Supplementary Tables S1 and S2, available at http://journals.cambridge.org/geo).

For quantitative spot analysis, the concentrations of most of the REE as well as the calculated Ce anomalies exhibit systematic variations in both the horizontal and vertical directions of the nodule (Fig. 6; online Supplementary Table S3). Specifically, Ce anomalies decrease gradually from the centre to the edge ($Ce/Ce^* = 0.8$ to 0.92), while the REE contents generally increase towards the rim. This feature is significant for light REE (LREE) and MREE, but is not significant for heavy REE (HREE). The PAAS-normalized REE patterns are characterized by striking MREE enrichments ($Dy_N/Sm_N = 0.61$ to 1.31), with no apparent variation along the transections (Figs 6, 7).

## 5. Discussion

### 5.a. Principal component analysis

Principal component analysis (PCA), which enables dimension reduction of multivariate datasets, is widely used to understand element enrichments and their governing processes in geological environments (e.g. Gregory *et al.* 2015; Ahm *et al.* 2017; Ye *et al.* 2020). PCA enables the investigation of how different variables vary with each other, and the grouping of them into principal components. The first component in our PCA model includes two groups: PC1 (Ca, P and Sr) and negative PC1 (Al, Si, Sc, Ti and Zr). The former represents carbonate fluorapatite (CFA), while the latter corresponds to detrital components of the black shale host, such as quartz, rutile, zircon and other silicate minerals. The comparable distributions of Sr and Ca indicate extensive substitution of

https://doi.org/10.1017/S0016756820000850 Published online by Cambridge University Press

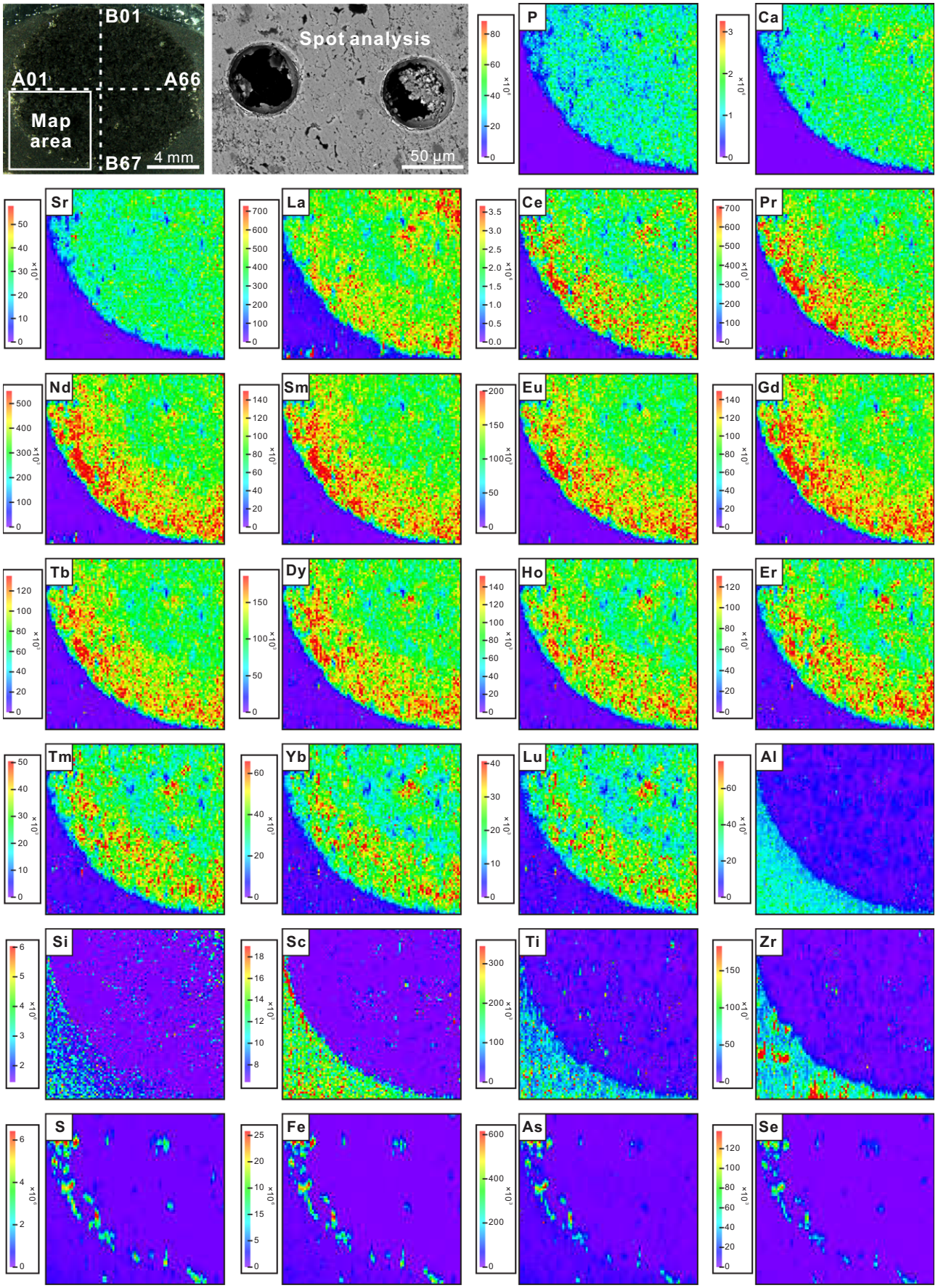


**Fig. 4.** (Colour online) Optic, electronic (BSE) and LA-ICP-MS images of the studied nodule. Note that the white dashed lines indicate the routes of spot analysis and the white box represents the mapping area. The scales of LA-ICP-MS images are counts-per-second (CPS).

https://doi.org/10.1017/S0016756820000850 Published online by Cambridge University Press

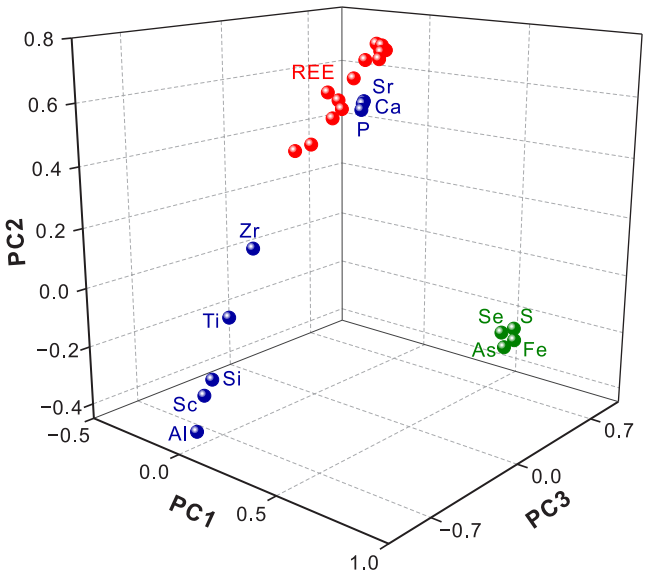


**Fig. 5.** (Colour online) Principal component analysis based on the raw LA-ICP-MS dataset.

$Sr^{2+}$ for $Ca^{2+}$ with no change in charge balance (Figs 4, 5; Chakhmouradian *et al.* 2017).

Component 2 consists of the entire REE series, which share very similar physical and chemical properties. This uniformity arises from the nature of their electronic configurations, resulting in a primarily stable oxidation state. The small differences in this set of elements can be attributed to a steady decrease in ionic radius with increasing atomic number (i.e. the lanthanide contraction). REE can reside in CFA through the substitution of $REE^{3+}$ for $Ca^{2+}$ or through direct attachment to crystal surface (Jarvis *et al.* 1994; Reynard *et al.* 1999). Fleet *et al.* (2000) found that both the ninefold-coordinated Ca1 site and the sevenfold-coordinated Ca2 site can accommodate significant amounts of REE. The REE signatures retained by CFA are believed to be critical for determining the environmental dynamics, as discussed in the following section.

Component 3 includes Fe, S, As and Se, which are typical elements within the structure of pyrite. In organic-rich deposits, syngenetic and diagenetic pyrites have been recognized as sinks of several trace metals (Large *et al.* 2014; Gregory *et al.* 2015). The incorporation of As into pyrite can occur in two different ways: (1) the substitution of $As^{-}$ for S in the S unit; or (2) the substitution of $As^{3+}$ for $Fe^{2+}$ (Reich & Becker, 2006; Deditius *et al.* 2008; Neumann *et al.* 2013). Selenium concentration of pyrite is primarily regulated by its substitution for S. Experimental studies have shown that up to 99.5% Se in solution could be taken up by pyrite precipitation, demonstrating the high affinity of Se for Fe sulphides (Diener *et al.* 2012). Notably, the pyrites formed around the periphery of our nodule are most likely the consequence of late-stage sulphate reduction and void filling (Fig. 3).

## 5.b. Interpretations of REE patterns

### 5.b.1. Ce anomaly

Cerium is the only REE that undergoes redox transformation under low-temperature conditions. The oxidation of dissolved $Ce^{3+}$ to form insoluble $Ce^{4+}$ takes place in the modern oxygenated water column through coating of organic matter and/or Mn–Fe oxides, resulting in lower Ce concentrations in the deep ocean relative to La and Pr, which is expressed as a negative Ce anomaly. Under reducing conditions, the insoluble $Ce^{4+}$ is converted back into soluble $Ce^{3+}$, which behaves similarly to the other REEs. In this case, little or no inter-element fractionation is identified (Elderfield & Sholkovitz, 1987; Moffett, 1990; Alibo & Nozaki, 1999; Bau & Koschinsky *et al.* 2009).

Since phosphate nodules grow beneath the sediment–water interface, it is reasonable to assume that the systematic variations in Ce/Ce* and the total REE contents (ΣREE) are the result of progressive diagenetic alternation. Shields & Stille (2001) proposed that the diagenetic reaction can be evaluated using plots of Ce/Ce* versus ΣREE and $Dy_N/Sm_N$ because diagenetic REE exchange with host sediments would erase the original negative Ce anomaly and induce greater REE enrichment and MREE arching. Accordingly, Ce/Ce* is expected to correlate positively with ΣREE and negatively with $Dy_N/Sm_N$. However, as shown in Figure 8, neither of these relationships was observed for the studied sample. Instead, there is a negative correlation between Ce/Ce* and ΣREE. If diagenesis did play a role in producing the elevated REE concentrations, the nodule rim, which underwent severe diagenetic addition of REE, should have more muted Ce anomalies compared with its core. Such a scenario contradicts our data, where the most prominent negative Ce anomaly is present in the rim concurrent with the relatively higher REE abundances (Fig. 6); other explanations for these variations are therefore required.

Based on observations of the modern environment, two hypotheses are proposed to account for the Ce/Ce* and ΣREE profiles of the nodule. First, we note that there could be a significant difference between the inner and outer parts in terms of the exposure time to pore water. As CFA crystallites grew, the inner part would be impermeable and more closed, while the outer part was still in contact with ambient fluid, resulting in the incorporation of REE into the rim (Ilyin 1998; Zhu *et al.* 2014). It should be emphasized that, unlike the late diagenetic modification discussed above, this process must occur at a very early stage when pore water was not completely isolated from seawater and possessed a prominent negative Ce anomaly. The outer zone, which experienced a stronger exchange with the pore water, therefore exhibits lower Ce/Ce* (i.e. is more oxygenated). This hypothesis also explains why the core-to-rim increasing trend is less pronounced for HREE than for LREE and MREE (Fig. 4; online Supplementary Table S3). REE mainly exist as carbonate complexes in seawater. The stability of REE – carbonate ion complexes and the opportunity for particulate adsorption vary inversely through the REE series (Koeppenkastrop & De Carlo, 1992; Sholkovitz, 1992; Sholkovitz *et al.* 1994). As a consequence, LREE and MREE with higher mobilities were preferentially bonded to the CFA surface, whereas HREE were retained in the solution.

Second, the changes in Ce/Ce* and ΣREE may be related to changes in the water depth. Modern coastal and marine surface waters generally have little or no negative Ce anomalies, but the Ce/Ce* values decrease steadily with increasing depth to form a more typical Ce deficit. The REE contents also exhibit systematic variations with increasing water depth (Alibo & Nozaki, 1999; Deng *et al.* 2017). The observed Ce anomalies are therefore considered to be a function of bathymetry. Importantly, this assumption holds true only if the pore water always had a good connection to the overlying seawater during precipitation of CFA.

### 5.b.2. MREE enrichment

Most of our analysed spots are markedly enriched in MREE (Fig. 7). Several models have been suggested to explain the mechanisms of this pattern. One possibility is that the MREE are

https://doi.org/10.1017/S0016756820000850 Published online by Cambridge University Press

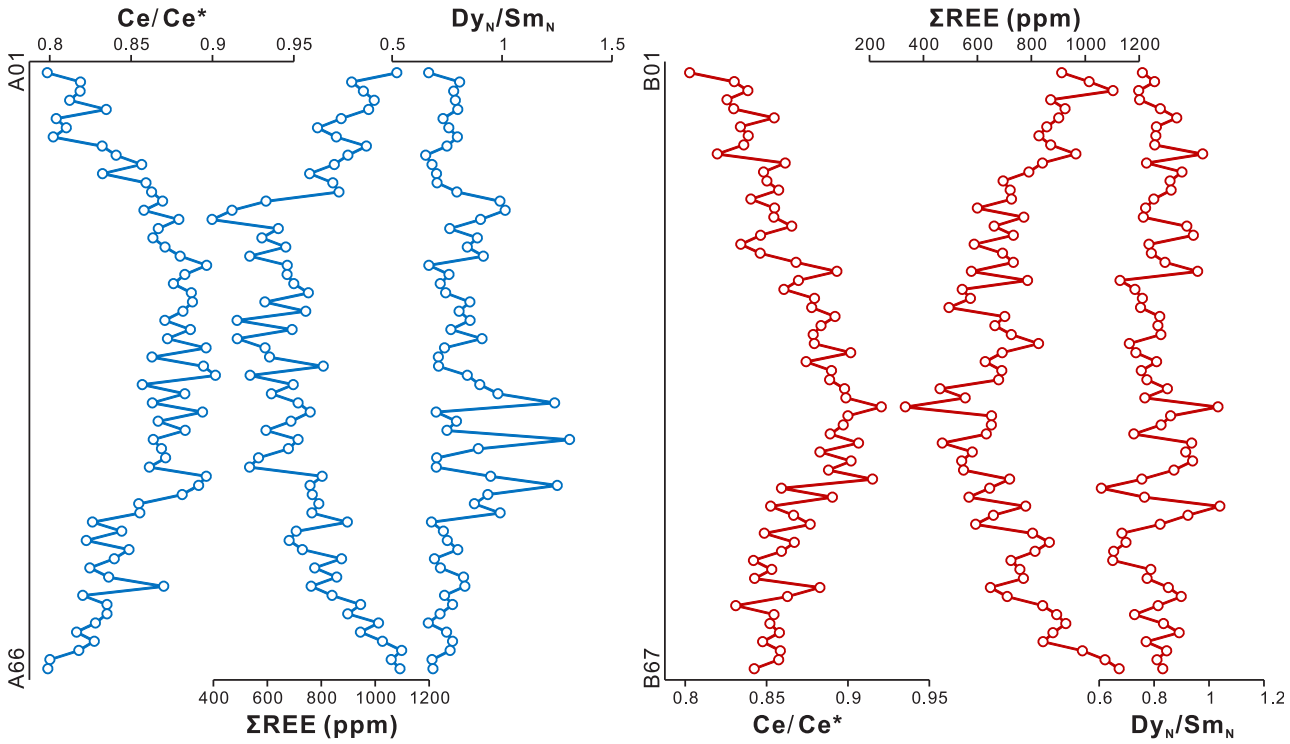


**Fig. 6.** (Colour online) Horizontal (A01–A66) and vertical (B01–B67) profiles of Ce/Ce*, ΣREE and $Dy_N/Sm_N$. See Figure 4 for trails of the spots.

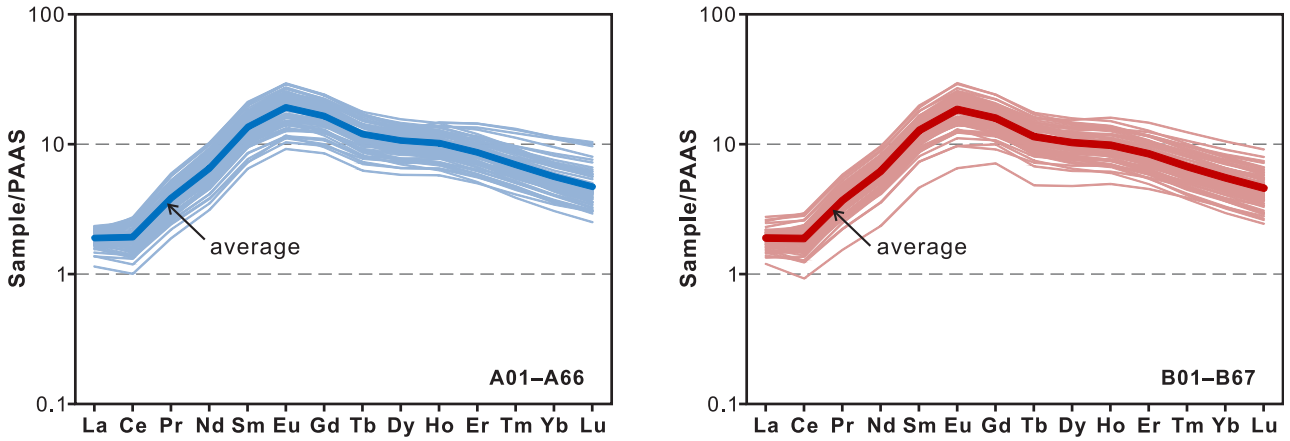


**Fig. 7.** (Colour online) PAAS-normalized REE patterns of phosphate nodule.

preferentially taken up and are substituted for Ca in the CFA lattice. The partition coefficients of the REE between apatite and melt exhibit a convex-upwards shape, indicating that apatite accommodates MREE more readily than LREE or HREE (Reynard *et al.* 1999; Klemme & Dalpé, 2003). However, seawater-like REE distributions are known to be preserved in many modern and ancient P-enriched deposits (Toyoda & Tokonami, 1990; Jiang *et al.* 2007; Zhu *et al.* 2014; Xin *et al.* 2015; Zhai *et al.* 2016); the substitution model alone may therefore not explain all of the MREE enrichments.

Another possibility is that this pattern represents the REE characteristics of organic matter. Several studies have revealed that organic colloids can dominate REE retention in aqueous systems (Elderfield *et al.* 1990; Sholkovitz, 1992; Stolpe *et al.* 2013). An extraction experiment by Freslon *et al.* (2014) demonstrated that sedimentary organic compounds from different environments share similar MREE-enriched patterns. The remineralization of organic particles in highly productive areas or during diagenesis is capable of imparting its signature to the dissolved load. Authigenic CFA precipitated in equilibrium with the evolved fluid would record the organic REE patterns accordingly. Based on the apparent black opaque appearance of our sample, the REE distributions are at least partially controlled by organic component. However, some organic-poor phosphorites from this time are also enriched in MREE (Xin *et al.* 2015; Zhu & Jiang, 2017), suggesting that there are other REE sources in addition to the organic matter. Furthermore, the REE compositions of kerogen in the Niutitang black shales show diverse patterns instead of a single MREE bulge, which might be related to different contributions of marine biomass (Pi *et al.* 2013).

https://doi.org/10.1017/S0016756820000850 Published online by Cambridge University Press

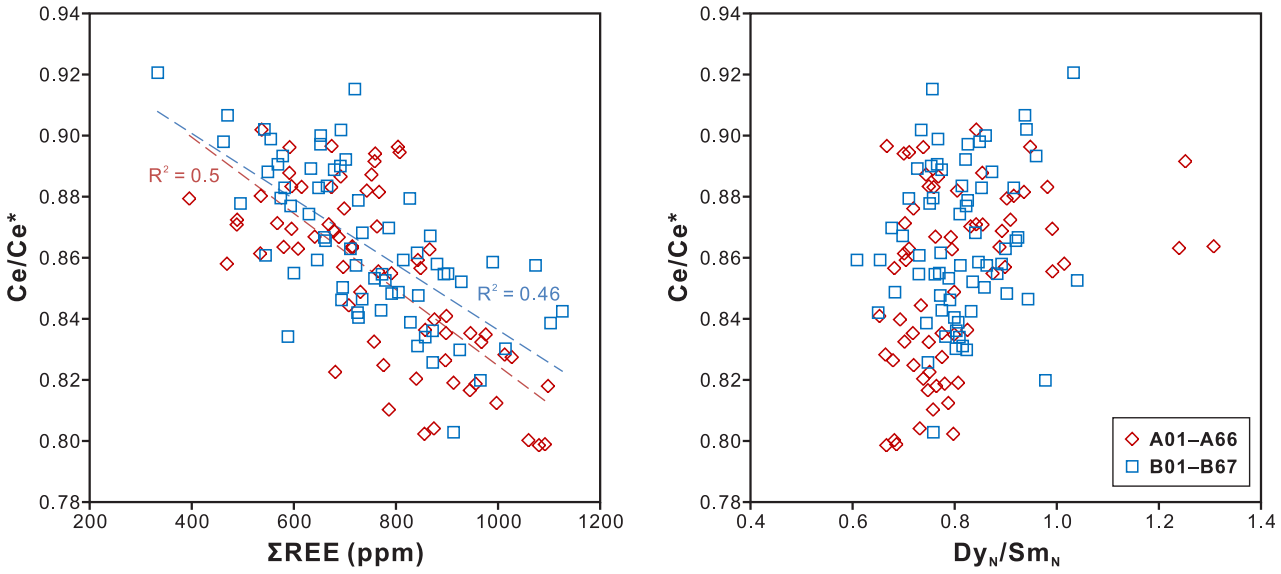


**Fig. 8.** (Colour online) Cross-plots of Ce/Ce* versus ΣREE and $Dy_N/Sm_N$.

The reduction of Fe oxides can also be a potential driver of elevated MREE concentrations. In sediments off the coast of Peru and on the California margin, the coincidence of pore water exhibiting the MREE bulge with the peak of dissolved Fe production suggests that Fe oxides are the carriers of this MREE signal (Johannesson & Zhou, 1999; Haley *et al.* 2004). Accordingly, MREE enrichment is sometimes considered to be the diagnostic pattern for ferruginous environments (e.g. Kim *et al.* 2012; Chen *et al.* 2015*b*; Ye *et al.* 2020). For example, MREE enrichments of the Mesoproterozoic Xiamaling carbonate concretions (Liu *et al.* 2019) and the Ediacaran Doushantuo cap carbonates (Wu *et al.* 2019) are both attributed to metal oxide reduction. Since carbonate samples generally have low TOC, it is reasonable to exclude organic matter as a candidate. But for our nodule, assigning the REE pattern to individual sources is still challenging. Future research, such as sequential leaching experiment, may provide new insights into the causes of such MREE enrichment pattern.

Interestingly, among these hypotheses regarding MREE enrichment, some researchers have speculated that seawater of pre-Cenozoic oceans was itself MREE-enriched (Grandjean-Lécuyer *et al.* 1993; Ilyin, 1998; Lécuyer *et al.* 2004; Emsbo *et al.* 2015). Ilyin (1998) found that almost all Proterozoic–Cambrian phosphorites have a so-called old-phosphorite REE type, which contains a negative Ce anomaly and remarkable HREE depletion. However, this secular variation idea was strongly criticized by Shields & Webb (2004), given that contemporaneous calcites have retained REE signals similar to the modern seawater pattern. They claimed that this HREE deficiency and other non-seawater-like features were likely derived from post-depositional exchange or non-quantitative uptake of REE.

Here, we propose that the conflicting views about seawater REE composition can be reconciled through a chemically stratified model (Fig. 9). A growing amount of evidence has demonstrated that Precambrian and early Cambrian oceans were characterized by extreme spatial heterogeneity and stratification (Li *et al.* 2010; Poulton *et al.* 2010; Jin *et al.* 2016; Zhang *et al.* 2016; Hammarlund *et al.* 2017). Because of the redox control on REE behaviour, the REE patterns of ancient seawater should be comparable to those of modern pore water, which has been verified to record discernible REE patterns within a fixed respiration sequence (i.e. oxic, nitrogenous, manganous, ferruginous, sulphidic and methanic; Haley *et al.* 2004; Canfield & Thamdrup, 2009; Kim *et al.* 2012; Li *et al.* 2015). Marine minerals precipitated in different locations of the ocean would therefore carry different REE signals (that is to say, the ferruginous condition mentioned above might not have been restricted to pore water). In the modern oceans, the massive sedimentation of carbonates occurs on tropical and subtropical continental shelves, referred to as the carbonate factory (Bosscher & Schlager, 1992). The REE distributions of these carbonates are inherited from the oxic surface waters. In contrast, the depositions of contemporaneous phosphorites are more constrained to marginal settings beneath highly productive upwelling currents (as discussed further in the following section), although some may suffer reworking and winnowing. With regard to early Cambrian oceans, such environments could be close to the oxygen-deficient manganous and/or ferruginous or even sulphidic zone (Pufahl & Hiatt, 2012). Indeed, the stratification of REE has been identified in oceans during Proterozoic to early Cambrian time (Planavsky *et al.* 2010; Hood & Wallace, 2015; Tostevin *et al.* 2016*b*; Wu *et al.* 2019). A fundamental change of marine redox state during late Phanerozoic time might have ultimately led to a uniform seawater REE pattern.

### 5.c. Mechanisms of phosphogenesis

The main realms of modern phosphorite formations are the major upwelling systems along continental margins, such as on the western coasts of Peru and Chile (Manheim *et al.* 1975; Burnett, 1977; Glenn & Arthur, 1988). The initial enrichments of P in these settings are orchestrated by a complex interplay between several processes, including organic matter degradation, Fe oxide pumping and microbial activity.

The role of microbes in phosphogenesis has particularly attracted the attention of scientists in recent years. For sediments beneath the Benguela upwelling area off the coast of Namibia, Schulz & Schulz (2005) reported the co-occurrence of a narrow horizon of CFA, a spike in the dissolved phosphate content and an aggregation of giant sulphide-oxidizing bacteria

https://doi.org/10.1017/S0016756820000850 Published online by Cambridge University Press

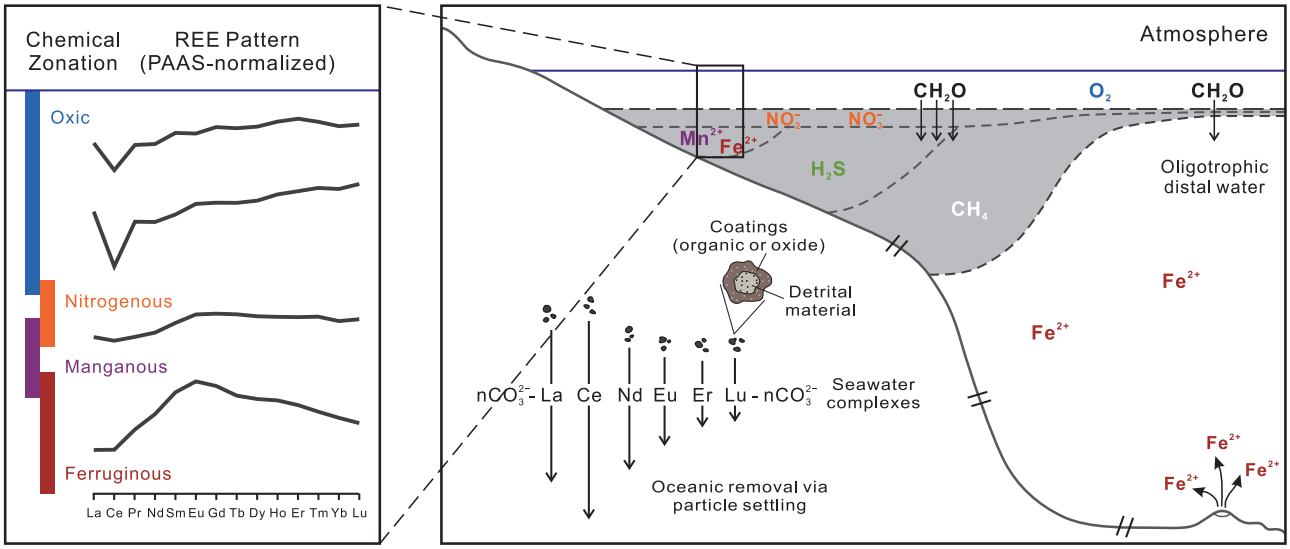


**Fig. 9.** (Colour online) A conceptual model for Precambrian and early Cambrian oceans (Canfield & Thamdrup, 2009; Li *et al.* 2015). The left panel represents the evolution of REE within different redox zones (modified from Deng *et al.* 2017).

*Thiomargarita namibiensis*. *T. namibiensis* is known to be capable of accumulating polyphosphate intracellularly under oxic conditions, then hydrolysing the polyphosphate and releasing phosphate when the surrounding water becomes anoxic (Schulz & Schulz, 2005). Moreover, Goldhammer *et al.* (2010) found that sulphide-oxidizing bacteria can collect $^{33}$P-labelled phosphate into their cells and catalyse nearly instantaneous conversion of phosphate to apatite. Brock & Schulz-Vogt (2011) investigated parameters that could stimulate the decomposition of polyphosphate in a marine *Beggiatoa* strain, and concluded that sulphide exposure would trigger phosphate release by *Beggiatoa*. Overall, under alternating oxic and anoxic regimes, sulphur bacteria appear to have a remarkable effect on focusing pore-water phosphate. Such a condition could easily have been achieved in Ediacaran–Cambrian oceans, in which oxidant supply and oxygen level were relatively unstable, fostering frequent redox oscillations, vigorous microbial activity and subsequent pore-water phosphate build-up.

Indeed, filamentous microfossils that resemble modern sulphide-oxidizing bacteria were reported from the Ediacaran Doushantuo Formation in South China (Bailey *et al.* 2013). These fossils contain opaque inclusions that represent putative relict S globules. Although such fossils are not observed in our nodule, their findings reflect that sulphur bacteria, which are known to mediate CFA precipitation in modern environments, might have been present in phosphogenic settings during the Ediacaran–Cambrian period.

## 6. Conclusions

In summary, the observed core-to-rim Ce/Ce* variations of a phosphate nodule from the basal part of the Niutitang Formation are interpreted to represent REE exchange with pore water at a very early stage or they might be correlated with increasing water depth during progressive growth of the nodule. The rare presence of pyrite within the nodule indicates that CFA was precipitated before extensive sulphate reduction. Causes of the MREE enrichment are still enigmatic. Potential mechanisms include preferential MREE substitution for Ca, degradation of organic matter and deposition under ferruginous environments. It is likely that the observed MREE patterns are the result of a combination of these mechanisms. Phosphate nodules deposited on continental margins during early Cambrian time were subject to a mid-depth chemical zonation with high organic loading from the surface waters. Such a scenario is consistent with the idea that transient redox switches can play an important role in phosphate accumulation.

**Supplementary Material.** To view supplementary material for this article, please visit https://doi.org/10.1017/S0016756820000850

**Acknowledgements.** We thank Fang Ma for laboratory assistance. Financial support was provided by the National Key Research and Development Program of China (2017YFC0603101), the National Science and Technology Major Project of the Ministry of Science and Technology of China (2016ZX05004001), the National Natural Science Foundation of China (41530317, 41872125), the Strategic Priority Research Program of the Chinese Academy of Sciences (XDA14010101) and the Scientific Research and Technological Development Project of CNPC (2016A-0200). This paper benefited greatly from the comments of Malcolm Wallace, Gerald Auer and an anonymous reviewer.

**Declaration of Interest.** The authors declare no competing interests.

## References

**Ahm A-SC, Bjerrum CJ and Hammarlund EU** (2017) Disentangling the record of diagenesis, local redox conditions, and global seawater chemistry during the latest Ordovician glaciation. *Earth and Planetary Science Letters* **459**, 145–56.

**Alibo DS and Nozaki Y** (1999) Rare earth elements in seawater: particle association, shale-normalization, and Ce oxidation. *Geochimica et Cosmochimica Acta* **63**, 363–72.

**Auer G, Reuter M, Hauzenberger CA and Piller WE** (2017) The impact of transport processes on rare earth element patterns in marine authigenic and biogenic phosphates. *Geochimica et Cosmochimica Acta* **203**, 140–56.

**Bailey JV, Corsetti FA, Greene SE, Crosby CH, Liu P and Orphan VJ** (2013) Filamentous sulfur bacteria preserved in modern and ancient phosphatic sediments: implications for the role of oxygen and bacteria in phosphogenesis. *Geobiology* **11**, 397–405.

**Bau M and Koschinsky A** (2009) Oxidative scavenging of cerium on hydrous Fe oxide: evidence from the distribution of rare earth elements and yttrium between Fe oxides and Mn oxides in hydrogenetic ferromanganese crusts. *Geochemical Journal* **43**, 37–47.

**Bosscher H and Schlager W** (1992) Computer simulation of reef growth. *Sedimentology* **39**, 503–12.

**Bright CA, Cruse, AM, Lyons TW, MacLeod KG, Glascock MD and Ethington RL** (2009) Seawater rare-earth element patterns preserved in apatite of Pennsylvanian conodonts? *Geochimica et Cosmochimica Acta* **73**, 1609–24.

**Brock J and Schulz-Vogt HN** (2011) Sulfide induces phosphate release from polyphosphate in cultures of a marine *Beggiatoa* strain. *The ISME Journal* **5**, 497–506.

**Burnett WC** (1977) Geochemistry and origin of phosphorite deposits from off Peru and Chile. *Geological Society of America Bulletin* **88**, 813–23.

**Canfield DE and Thamdrup B** (2009) Towards a consistent classification scheme for geochemical environments, or, why we wish the term 'suboxic' would go away. *Geobiology* **7**, 385–92.

**Chakhmouradian AR, Reguir EP, Zaitsev AN, Couëslan C, Xu C, Kynický J, Mumin AH and Yang P** (2017) Apatite in carbonatitic rocks: compositional variation, zoning, element partitioning and petrogenetic significance. *Lithos* **274–275**, 188–213.

**Chen D, Wang J, Qing H, Yan D and Li R** (2009) Hydrothermal venting activities in the Early Cambrian, South China: petrological, geochronological and stable isotopic constraints. *Chemical Geology* **258**, 168–81.

**Chen D, Zhou X, Fu Y, Wang J and Yan D** (2015a) New U–Pb zircon ages of the Ediacaran–Cambrian boundary strata in South China. *Terra Nova* **27**, 62–8.

**Chen J, Algeo TJ, Zhao L, Chen Z-Q, Cao L, Zhang L and Li Y** (2015b) Diagenetic uptake of rare earth elements by bioapatite, with an example from Lower Triassic conodonts of South China. *Earth-Science Reviews* **149**, 181–202.

**Deditius AP, Utsunomiya S, Renock D, Ewing RC, Ramana CV, Becker U and Kesler SE** (2008) A proposed new type of arsenian pyrite: composition, nanostructure and geological significance. *Geochimica et Cosmochimica Acta* **72**, 2919–33.

**Deng Y, Ren J, Guo Q, Cao J, Wang H and Liu C** (2017) Rare earth element geochemistry characteristics of seawater and porewater from deep sea in western Pacific. *Scientific Reports* **7**, 16539.

**Diener A, Neumann T, Kramar U and Schild D** (2012) Structure of selenium incorporated in pyrite and mackinawite as determined by XAFS analyses. *Journal of Contaminant Hydrology* **133**, 30–9.

**Elderfield H and Sholkovitz ER** (1987) Rare earth elements in the pore waters of reducing nearshore sediments. *Earth and Planetary Science Letters* **82**, 280–8.

**Elderfield H, Upstill-Goddard R and Sholkovitz ER** (1990) The rare earth elements in rivers, estuaries, and coastal seas and their significance to the composition of ocean waters. *Geochimica et Cosmochimica Acta* **54**, 971–91.

**Emsbo P, McLaughlin PI, Breit GN, du Bray EA and Koenig AE** (2015) Rare earth elements in sedimentary phosphate deposits: solution to the global REE crisis? *Gondwana Research* **27**, 776–85.

**Fleet ME, Liu X and Pan Y** (2000) Rare-earth elements in chlorapatite $[Ca_{10}(PO_4)_6Cl_2]$: uptake, site preference and degradation of monoclinic structure. *American Mineralogist* **85**, 1437–46.

**Freslon N, Bayon G, Toucanne S, Bermell S, Bollinger C, Chéron S, Etoubleau J, Germain Y, Khripounoff A, Ponzevera E and Rouget M-L** (2014) Rare earth elements and neodymium isotopes in sedimentary organic matter. *Geochimica et Cosmochimica Acta* **140**, 177–98.

**Glenn CR and Arthur MA** (1988) Petrology and major element geochemistry of Peru margin phosphorites and associated diagenetic minerals: authigenesis in modern organic-rich sediments. *Marine Geology* **80**, 231–67.

**Goldhammer T, Brüchert V, Ferdelman TG and Zabel M** (2010) Microbial sequestration of phosphorus in anoxic upwelling sediments. *Nature Geoscience* **3**, 557–61.

**Grandjean-Lécuyer P, Feist R and Albarède F** (1993) Rare earth elements in old biogenic apatites. *Geochimica et Cosmochimica Acta* **57**, 2507–14.

**Gregory DD, Large RR, Halpin JA, Lounejeva Baturina E, Lyons TW, Wu S, Danyushevsky L, Sack PJ, Chappaz A, Maslennikov VV and Bull SW** (2015) Trace element content of sedimentary pyrite in black shales. *Economic Geology* **110**, 1389–410.

**Haley BA, Klinkhammer GP and McManus J** (2004) Rare earth elements in pore waters of marine sediments. *Geochimica et Cosmochimica Acta* **68**, 1265–79.

**Hammarlund EU, Gaines RR, Prokopenko MG, Qi C, Hou X-G and Canfield DE** (2017) Early Cambrian oxygen minimum zone-like conditions at Chengjiang. *Earth and Planetary Science Letters* **475**, 160–68.

**Hood AVS and Wallace MW** (2015) Extreme ocean anoxia during the Late Cryogenian recorded in reefal carbonates of Southern Australia. *Precambrian Research* **261**, 96–111.

**Horan MF, Morgan JW, Grauch RI, Coveney RM, Murowchick JB and Hulbert LJ** (1994) Rhenium and osmium isotopes in black shales and Ni-Mo-PGE-rich sulfide layers, Yukon Territory, Canada, and Hunan and Guizhou provinces, China. *Geochimica et Cosmochimica Acta* **58**, 257–65.

**Ilyin AV** (1998) Rare-earth geochemistry of 'old' phosphorites and probability of syngenetic precipitation and accumulation of phosphate. *Chemical Geology* **144**, 243–56.

**Jarvis I, Burnett W, Nathan Y, Almbaydin F, Attia A, Castro L, Flicoteaux R, Hilmy ME, Husain V and Qutawnah A** (1994) Phosphorite geochemistry: state-of-the-art and environmental concerns. *Eclogae Geologicae Helvetiae* **87**, 643–700.

**Jiang S-Y, Pi D-H, Heubeck C, Frimmel H, Liu Y-P, Deng H-L, Ling H-F and Yang J-H** (2009) Early Cambrian ocean anoxia in South China. *Nature* **459**, E5–6.

**Jiang S-Y, Zhao H-X, Chen Y-Q, Yang T, Yang J-H and Ling H-F** (2007) Trace and rare earth element geochemistry of phosphate nodules from the lower Cambrian black shale sequence in the Mufu Mountain of Nanjing, Jiangsu province, China. *Chemical Geology* **244**, 584–604.

**Jin C, Li C, Algeo TJ, Planavsky NJ, Cui H, Yang X, Zhao Y, Zhang X and Xie S** (2016) A highly redox-heterogeneous ocean in South China during the early Cambrian (~529–514 Ma): implications for biota-environment co-evolution. *Earth and Planetary Science Letters* **441**, 38–51.

**Johannesson KH and Zhou X** (1999) Origin of middle rare earth element enrichments in acid waters of a Canadian High Arctic lake. *Geochimica et Cosmochimica Acta* **63**, 153–65.

**Kim J-H, Torres ME, Haley BA, Kastner M, Pohlman JW, Riedel M and Lee Y-J** (2012) The effect of diagenesis and fluid migration on rare earth element distribution in pore fluids of the northern Cascadia accretionary margin. *Chemical Geology* **291**, 152–65.

**Klemme S and Dalpé C** (2003) Trace-element partitioning between apatite and carbonatite melt. *American Mineralogist* **88**, 639–46.

**Koeppenkastrop D and De Carlo EH** (1992) Sorption of rare-earth elements from seawater onto synthetic mineral particles: an experimental approach. *Chemical Geology* **95**, 251–63.

**Large RR, Halpin JA, Danyushevsky LV, Maslennikov VV, Bull SW, Long JA, Gregory DD, Lounejeva E, Lyons TW, Sack PJ, McGoldrick PJ and Calver CR** (2014) Trace element content of sedimentary pyrite as a new proxy for deep-time ocean–atmosphere evolution. *Earth and Planetary Science Letters* **389**, 209–20.

**Lawrence MG, Greig A, Collerson KD and Kamber BS** (2006) Rare earth element and yttrium variability in South East Queensland waterways. *Aquatic Geochemistry* **12**, 39–72.

**Lécuyer C, Reynard B and Grandjean P** (2004) Rare earth element evolution of Phanerozoic seawater recorded in biogenic apatites. *Chemical Geology* **204**, 63–102.

**Lehmann B, Frei R, Xu L and Mao J** (2016) Early Cambrian black shale-hosted Mo-Ni and V mineralization on the rifted margin of the Yangtze platform, China: reconnaissance chromium isotope data and a refined metallogenic model. *Economic Geology* **111**, 89–103.

**Li C, Cheng M, Algeo TJ and Xie SC** (2015) A theoretical prediction of chemical zonation in early oceans (>520 Ma). *Science China Earth Sciences* **58**, 1901–09.

**Li C, Love GD, Lyons TW, Fike DA, Sessions AL and Chu X** (2010) A stratified redox model for the Ediacaran ocean. *Science* **328**, 80–3.

**Liu A-Q, Tang D-J, Shi X-Y, Zhou L-M, Zhou X-Q, Shang M-H, Li Y and Song H-Y** (2019) Growth mechanisms and environmental implications of carbonate concretions from the ~1.4 Ga Xiamaling Formation, North China. *Journal of Palaeogeography* **8**, 285–300.

**Manheim F, Rowe G and Jipa D** (1975) Marine phosphorite formation off Peru. *Journal of Sedimentary Petrology* **45**, 243–51.

**Mao JW, Lehmann B, Du AD, Zhang GD, Ma DS, Wang YT, Zeng MG and Kerrich R** (2002) Re-Os dating of polymetallic Ni-Mo-PGE-Au

https://doi.org/10.1017/S0016756820000850 Published online by Cambridge University Press

mineralization in lower Cambrian black shales of south China and its geologic significance. *Economic Geology* **97**, 1051–61.

**McKerrow WS, Scotese CR and Brasier MD** (1992) Early Cambrian continental reconstructions. *Journal of the Geological Society of London* **149**, 599–606.

**Moffett JW** (1990) Microbially mediated cerium oxidation in sea water. *Nature* **345**, 421–3.

**Neumann T, Scholz F, Kramar U, Ostermaier M, Rausch N, Berner Z and Immenhauser A** (2013) Arsenic in framboidal pyrite from recent sediments of a shallow water lagoon of the Baltic Sea. *Sedimentology* **60**, 1389–404.

**Pi D-H, Liu C-Q, Shields-Zhou GA and Jiang S-Y** (2013) Trace and rare earth element geochemistry of black shale and kerogen in the early Cambrian Niutitang Formation in Guizhou province, South China: constraints for redox environments and origin of metal enrichments. *Precambrian Research* **225**, 218–29.

**Planavsky N, Bekker A, Rouxel OJ, Kamber B, Hofmann A, Knudsen A and Lyons TW** (2010) Rare Earth Element and yttrium compositions of Archean and Paleoproterozoic Fe formations revisited: new perspectives on the significance and mechanisms of deposition. *Geochimica et Cosmochimica Acta* **74**, 6387–405.

**Poulton SW, Fralick PW and Canfield DE** (2010) Spatial variability in oceanic redox structure 1.8 billion years ago. *Nature Geoscience* **3**, 486–90.

**Pufahl PK and Hiatt EE** (2012) Oxygenation of the Earth's atmosphere–ocean system: a review of physical and chemical sedimentologic responses. *Marine and Petroleum Geology* **32**, 1–20.

**Reich M and Becker U** (2006) First-principles calculations of the thermodynamic mixing properties of arsenic incorporation into pyrite and marcasite. *Chemical Geology* **225**, 278–90.

**Reynard B, Lecuyer C and Grandjean P** (1999) Crystal-chemical controls on rare-earth element concentrations in fossil biogenic apatites and implications for paleoenvironmental reconstructions. *Chemical Geology* **155**, 233–41.

**Schulz HN and Schulz HD** (2005) Large sulfur bacteria and the formation of phosphorite. *Science* **307**, 416–18.

**Shields G and Stille P** (2001) Diagenetic constraints on the use of cerium anomalies as palaeoseawater redox proxies: an isotopic and REE study of Cambrian phosphorites. *Chemical Geology* **175**, 29–48.

**Shields GA and Webb GE** (2004) Has the REE composition of seawater changed over geological time? *Chemical Geology* **204**, 103–07.

**Sholkovitz ER** (1992) Chemical evolution of rare earth elements: fractionation between colloidal and solution phases of filtered river water. *Earth and Planetary Science Letters* **114**, 77–84.

**Sholkovitz ER, Landing WM and Lewis BL** (1994) Ocean particle chemistry: the fractionation of rare earth elements between suspended particles and seawater. *Geochimica et Cosmochimica Acta* **58**, 1567–79.

**Steiner M, Li G, Qian Y, Zhu M and Erdtmann B-D** (2007) Neoproterozoic to early Cambrian small shelly fossil assemblages and a revised biostratigraphic correlation of the Yangtze Platform (China). *Palaeogeography, Palaeoclimatology, Palaeoecology* **254**, 67–99.

**Stolpe B, Guo L and Shiller AM** (2013) Binding and transport of rare earth elements by organic and iron-rich nanocolloids in Alaskan rivers, as revealed by field-flow fractionation and ICP-MS. *Geochimica et Cosmochimica Acta* **106**, 446–62.

**Taylor SR and McLennan SM** (1985) *The Continental Crust: Its Composition and Evolution*. Oxford: Blackwell Scientific Publications, 312 pp.

**Tostevin R, Shields GA, Tarbuck GM, He T, Clarkson MO and Wood RA** (2016a) Effective use of cerium anomalies as a redox proxy in carbonate-dominated marine settings. *Chemical Geology* **438**, 146–62.

**Tostevin R, Wood RA, Shields GA, Poulton SW, Guilbaud R, Bowyer F, Penny AM, He T, Curtis A, Hoffmann KH and Clarkson MO** (2016b) Low-oxygen waters limited habitable space for early animals. *Nature Communications* **7**, 12818.

**Toyoda K and Tokonami M** (1990) The diffusion of rare-earth elements in fish teeth from deep-sea sediments. *Nature* **345**, 607–9.

**Wallace MW, Hood AVS, Shuster A, Greig A, Planavsky NJ and Reed CP** (2017) Oxygenation history of the Neoproterozoic to early Phanerozoic and the rise of land plants. *Earth and Planetary Science Letters* **466**, 12–19.

**Wang H-J, Zhang S-C, Ye Y-T, Wang X-M, Zhou W-X and Su J** (2016) *In situ* imaging of multi-elements on pyrite using laser ablation-inductively coupled plasma-mass spectrometry. *Chinese Journal of Analytical Chemistry* **44**, 1665–70.

**Wang J and Li Z-X** (2003) History of Neoproterozoic rift basins in South China: implications for Rodinia break-up. *Precambrian Research* **122**, 141–58.

**Wang X, Shi X, Jiang G and Zhang W** (2012) New U–Pb age from the basal Niutitang Formation in South China: implications for diachronous development and condensation of stratigraphic units across the Yangtze platform at the Ediacaran–Cambrian transition. *Journal of Asian Earth Sciences* **48**, 1–8.

**Wu H-P, Jiang S-Y, Palmer MR, Wei H-Z and Yang J-H** (2019) Positive cerium anomaly in the Doushantuo cap carbonates from the Yangtze platform, South China: implications for intermediate water column manganous conditions in the aftermath of the Marinoan glaciation. *Precambrian Research* **320**, 93–110.

**Xin H, Jiang S-Y, Yang J-H, Wu H-P and Pi D-H** (2015) Rare earth element and Sr–Nd isotope geochemistry of phosphatic rocks in Neoproterozoic Ediacaran Doushantuo Formation in Zhangcunping section from western Hubei Province, South China. *Palaeogeography, Palaeoclimatology, Palaeoecology* **440**, 712–24.

**Xu L, Lehmann B, Mao J, Qu W and Du A** (2011) Re–Os age of polymetallic Ni–Mo–PGE–Au mineralization in Early Cambrian black shales of South China—a reassessment. *Economic Geology* **106**, 511–22.

**Ye Y, Wang H, Wang X, Zhai L, Wu C and Zhang S** (2020) Elemental geochemistry of lower Cambrian phosphate nodules in Guizhou Province, South China: an integrated study by LA-ICP-MS mapping and solution ICP-MS. *Palaeogeography, Palaeoclimatology, Palaeoecology* **538**, 109459.

**Yeasmin R, Chen D, Fu Y, Wang J, Guo Z and Guo C** (2017) Climatic-oceanic forcing on the organic accumulation across the shelf during the Early Cambrian (Age 2 through 3) in the mid-upper Yangtze Block, NE Guizhou, South China. *Journal of Asian Earth Sciences* **134**, 365–86.

**Zhai L, Wu C, Ye Y, Zhang S and An Z** (2016) Marine redox variations during the Ediacaran–Cambrian transition on the Yangtze Platform, South China. *Geological Journal* **53**, 58–79.

**Zhang S, Wang X, Wang H, Bjerrum CJ, Hammarlund EU, Costa MM, Connelly JN, Zhang B, Su J and Canfield DE** (2016) Sufficient oxygen for animal respiration 1,400 million years ago. *Proceedings of the National Academy of Sciences of the United States of America* **113**, 1731–36.

**Zhou W, Wang H, Fu Y, Ye Y, Wang X, Su J, Wang F, Ge Z, Liang H and Wei S** (2017) Study on the formation mechanism of phosphate nodules in the early Cambrian period using LA-ICP-MS multi-element imaging technology. *Rock and Mineral Analysis* **36**, 97–106 (in Chinese with English abstract).

**Zhu B and Jiang S-Y** (2017) A LA-ICP-MS analysis of rare earth elements on phosphatic grains of the Ediacaran Doushantuo phosphorite at Weng'an, South China: implication for depositional conditions and diagenetic processes. *Geological Magazine* **154**, 1381–97.

**Zhu B, Jiang S-Y, Yang J-H, Pi D, Ling H-F and Chen Y-Q** (2014) Rare earth element and Sr–Nd isotope geochemistry of phosphate nodules from the lower Cambrian Niutitang Formation, NW Hunan Province, South China. *Palaeogeography, Palaeoclimatology, Palaeoecology* **398**, 132–43.

**Zhu C, Wang H, Ye Y, Wang X, Huang J, Zhu Y and Yang R** (2019) The formation mechanism and geological significance of graptolite from the Longmaxi Formation: constraints from in situ multi-element imaging analysis. *Rock and Mineral Analysis* **38**, 245–59 (in Chinese with English abstract).